DOI: 10.1002/chem.201201321

Facile Synthesis of Fluorine-Substituted Benzothiadiazole-Based Organic Semiconductors and Their Use in Solution-Processed Small-Molecule Organic Solar Cells

Nara Cho,[a] Kihyung Song,[b] Jae Kwan Lee,*[c] and Jaejung Ko*[a]

Abstract: A facile new protocol for the synthesis of iodinated derivatives of fluorinated benzothiadiazoles is demonstrated for the production of p-type semiconducting materials. The newly synthesized small-molecule compounds **bis[TPA-diTh]-MonoF-BT** and **bis[TPA-diTh]-DiF-BT** exhibited a power conversion efficiency of 2.95 % and a high open-circuit voltage of 0.85 V in solution-processed small-molecule organic solar cells.

Keywords: charge transfer • halogenation • heterocycles • semiconductors • solar cells

Introduction

Solution-processed organic solar cells (OSCs) can be fabricated by versatile printing techniques such as doctor blade, inkjet, and roll-to-roll to provide inexpensive and lightweight devices. Over the last few years, efforts have been intensively focused on improving device performance toward achievement of a power conversion efficiency (PCE) of 10 %. Research has mainly been concerned with further developments in photoactive materials such as π-conjugated (semiconducting) polymer and fullerene derivatives, or functional layers such as buffering, charge transporting, and optical spacing layers.[1] Recently, the significant achievement of promising PCEs above 8 % for OSCs has provided opportunities for them to become strong candidates for next-generation solar cells, over inorganic thin-film solar cells and dye-sensitized solar cells (DSSCs).[2] Most of the reported high efficiencies have been demonstrated for OSCs fabricated with bulk-heterojunction (BHJ) materials comprising low-bandgap semiconducting polymers and [6,6]-phenyl-$C_{61(\text{or }71)}$-butyric acid methyl ester ($C_{61(\text{or }71)}$-PCBM).[3,7] Nevertheless, small-molecule chromophores have several advantages over their polymeric counterparts from the viewpoint of mass production for commercial application, on account of the low reproducibility of the polymers in terms of weight average molecular weight and polydispersity index, in addition to difficulties associated with purification. Hence, considerable research effort has focused on developing efficient small-molecule materials for improved device performance, with the near-term goal being a PCE comparable to that of polymer-based solar cells (PSCs).[4] Indeed, recent breakthroughs in achieving PCEs greater than 6 % have placed solution-processed small-molecule organic solar cells (SMOSCs) squarely in competition with PSCs.[5]

Efficient organic semiconductors reported for use in SMOSCs often have structural core motifs[4] such as oligothiophene, bridged dithiophene, benzothiadiazole (BT), squaraine, or diketopyrrolopyrrole. Their use is motivated by low-bandgap semiconducting polymers or push–pull molecular structures in nonlinear optics and DSSCs owing to their superior optoelectronic properties. Recently, we reported various symmetric and unsymmetric push–pull chromophores for solution-processed SMOSCs.[6] The use of push–pull structures in SMOSCs enables efficient intramolecular charge transfer (ICT), providing better molar absorptivity and the low bandgap required for an organic semiconductor. In addition, an electron-donating group such as triphenylamine (TPA) can play an important role in stabilizing the separated hole from an exciton and improving the hole-transporting properties of the hole carrier.[4,6] Recently, fluorine-substituted benzothiadiazole motifs were reported as effective electron-accepting units, producing a low-bandgap semiconducting PSC with 5–7 % efficiency.[7–9] The fluorine atom often affords unique features that, when integrated into a BHJ composite with PCBM, boosts intermolecular charge transfer through C−F⋯H interactions and thus affects the performance characteristics. For these reasons, we are interested in the more reinforced ICT from small-molecule organic semiconductors through substitution of an elec-

---

[a] N. Cho, Prof. J. Ko
Department of New Materials Chemistry
Korea University
Chungnam, 330-700 (Republic of Korea)
Fax: (+82) 41-860-5396
E-mail: jko@korea.ac.kr

[b] Prof. K. Song
Department of Chemical Education
Korea National University of Education
Chungbuk, 363-791 (Republic of Korea)

[c] Prof. J. K. Lee
Department of Chemistry Education
Chosun University
Gwangju, 501-759 (Republic of Korea)
Fax: (+82) 62-232-8122
E-mail: chemedujk@chosun.ac.kr

Supporting information for this article is available on the WWW under http://dx.doi.org/10.1002/chem.201201321.

tron-withdrawing atom, specifically fluorine, into the efficient push–pull semiconductor backbone for solution-processed SMOSCs.

Herein, we report the synthesis and photovoltaic characteristics of novel fluorine-substituted benzothiadiazole-based small-molecule compounds 2,6-bis(5,5′-bis(*N*,*N*′-diphenylaniline)-2,2′-bithiophenyl)-4,7-(5-fluorobenzo[*c*][1,2,5]thiadiazole) (**bis[TPA-diTh]-MonoF-BT**, **2**) and bis[5,5′-bis(*N*,*N*′-diphenylaniline)-2,2′-bithiophenyl]-4,7-(5,6-difluorobenzo[*c*]-[1,2,5]thiadiazole) (**bis[TPA-diTh]-DiF-BT**, **3**) as efficient p-type organic semiconductors in solution-processed SMOSCs. These compounds, in which mono- or difluorinated benzothiadiazole cores are linked with a electron-donating TPA group through a π-conjugated bithiophene bridge, gave PCEs of 2.95 % with a high open-circuit voltage (V_{oc}) of 0.85 V. They are compared with unfluorinated bis[5,5′-bis(*N*,*N*′-diphenylaniline)-2,2′-bithiophenyl]-4,7-benzo[*c*][1,2,5]thiadiazole (**bis[TPA-diTh]-BT**, **1**) (Scheme 1).

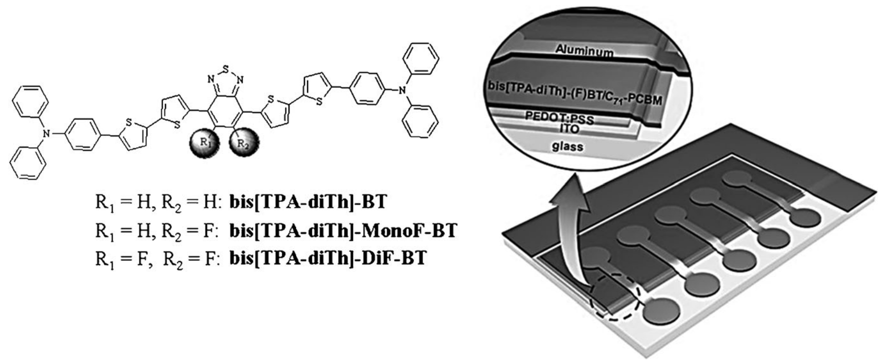

Scheme 1. Molecular structures of fluorinated **bis[TPA-diTh]-BT** derivatives and device architecture of solution-processed small-molecule organic solar cell.

Results and Discussion

The synthetic methods are outlined in Scheme 2. 5,6-Difluorobenzo[*c*][1,2,5]thiadiazole (**ii**) and *N*,*N*-diphenyl-4-(thiophen-2-yl)aniline were synthesized according to a previously reported procedure.[7,10] All reactions were carried out under a nitrogen atmosphere.

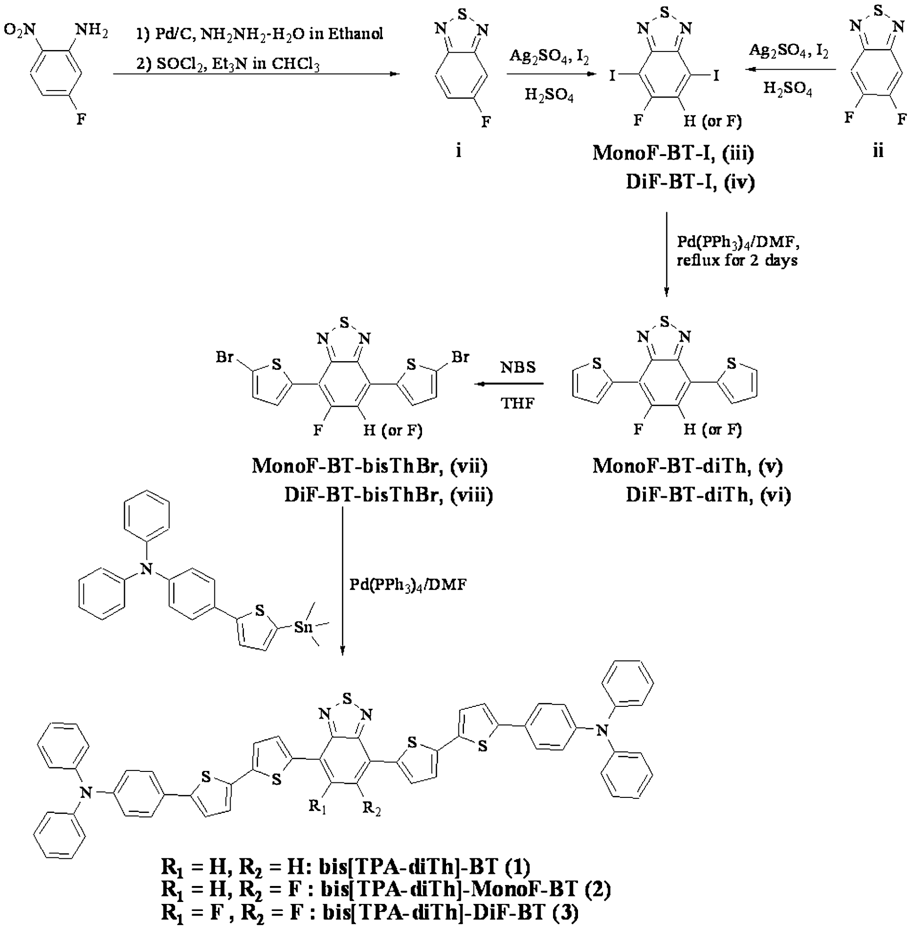

Scheme 2. Synthesis of the fluorinated **bis[TPA-diTh]-BT** derivatives.

Monofluorinated benzothiadiazole **MonoF-BT** (**i**) was readily prepared from its precursor by hydrogenation with Pd/C and hydrazine hydrate in absolute ethanol and subsequent cyclization with $SOCl_2$. Next, halogenation of the 4- and 7-positions of BT was carried out to facilitate the Stille coupling reaction with a stannyl BT. Recently, Zhou et al.[7] reported a synthetic approach for iodination of the 4- and 7-positions of difluorinated BT by using fuming sulfuric acid. Zhang et al. reported on bromination of mono- or difluorinated BT at the 4- and 7-positions using less hazardous reagents than Zhou et al., obtaining compounds **i** and **ii** in six synthetic steps.[8] The obvious benefits of a synthetic strategy using milder reagents and fewer steps than these methods led us to develop a facile new protocol for producing mono- or difluorinated BT iodinated at the 4- and 7-positions. The syntheses were performed successfully in a single-step reaction by using the Barker–Waters procedure. This involved the use of Ag_2SO_4 and I_2 in concentrated H_2SO_4 at 110 °C,[11] giving products **iii** and **iv** in yields of more than 65 %. The strong I^+ reagent is needed owing to the electron-deficient character of fluorinated BT.[12] Compounds **iii** and **iv** were converted to dithiophenyl compounds **v** and **vi**, respectively, by a Stille coupling reaction with $[Pd(PPh_3)_4]$ catalyst in *N*,*N*-dimethylformamide. Final compounds **2** and **3** were prepared by a Stille coupling reaction between electron-deficient fluorinated BT compounds **vii** and **viii** and stannyl TPA-thiophene. To clarify the effects of fluorine substitution on the electron-accepting BT core of these p-type organic semiconductors for SMOSCs, the unfluorinated BT derivative **1**[13] was also prepared by modifying the procedure.

Figure 1 shows the UV/Vis absorption spectra of **1–3** in chlorobenzene solution and thin films, and the corresponding optical properties are summarized in Table 1. The absorption spectra of **1–3** in chlorobenzene showed two typical transition bands in the wavelength region of 300–700 nm. The absorption bands observed at longer wavelengths result from ICT originating in HOMO→LUMO monoexcitations. The absorption bands observed at 300–500 nm could be assigned to the π–π* transition, which predominantly originates in HOMO−2→LUMO excitation (f=0.06–0.10) with minor HOMO−1→LUMO monoexcitations (f=0.02–0.06), showing very high oscillator strength (f) of transition. Time-dependent DFT calculations with the B3LYP functional/6-31G* basis set provided more information on these transition bands (see Table S1 in the Supporting Information).

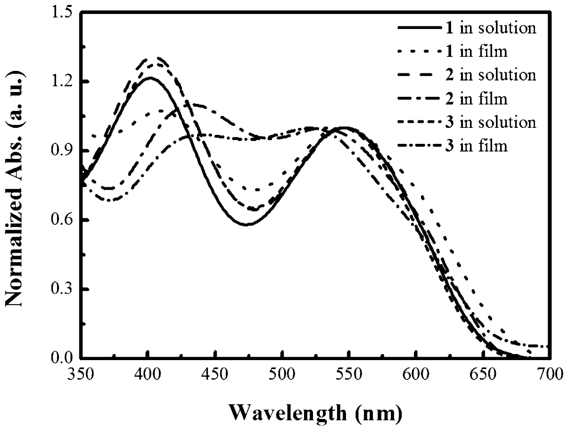

Figure 1. UV/Vis absorption spectra of **1–3** in chlorobenzene solution (**1**: solid line, **2**: dashed line, **3**: short-dashed line) and thin films (**1**: dotted line, **2**: dash-dotted line, **3**: short-dash-dotted line).

Table 1. Optical and electrochemical properties of the **bis[TPA-diTh]-BT** series.

Compound	λ_{abs} [nm][a] [ε $M^{-1}cm^{-1}$]	$E_{onset,ox}$ [V]/HOMO [eV][b]	$E_{onset,red}$ [V]/LUMO [eV][b]	$E_g^{electro}$ [eV][b]	E_g^{opt} [eV][c]
1	546 (54 000)	0.252/−5.052	−1.114/−3.686	1.366	1.85
2	547 (58 000)	0.273/−5.073	−1.116/−3.684	1.389	1.85
3	546 (57 900)	0.288/−5.088	−1.119/−3.681	1.407	1.85

[a] Absorption spectra were measured in chlorobenzene solution. [b] Redox potentials were measured in CH_2Cl_2 with 0.1 M $(n\text{-}C_4H_9)_4NPF_6$ and a scan rate of 100 mV s^{-1}. [c] E_g^{opt} was calculated from the absorption thresholds from absorption spectra in chlorobenzene solution.

Compounds **1–3** showed high molar absorption coefficients of 54 000 $M^{-1}cm^{-1}$ at 546 nm, 58 000 $M^{-1}cm^{-1}$ at 547 nm, and 57 900 $M^{-1}cm^{-1}$ at 545 nm, respectively. Fluorinated **bis[TPA-diTh]-BT** derivatives **2** and **3** exhibited higher molar absorptivities than the unfluorinated counterpart **1**, which indicated a more strongly reinforced ICT from TPA to the BT core. However, the reinforced ICT did not induce a redshift of the transition bands of **2** or **3**, perhaps because fluorination of the BT core slightly increased the energy bandgap between the HOMO and the LUMO by reducing the HOMO levels of **bis[TPA-diTh]-BT** derivatives **2** and **3** (see below).

In solid-state thin films, π-conjugated organic materials often show redshifted absorption bands and broader spectra relative to those in solution owing to intermolecular π–π packing interactions.[14] However, Figure 1 shows that **1** exhibited only spectral broadening, with no evident band shift to a longer wavelength region. This is likely caused by the amorphous nonplanar TPA, which may interrupt the intermolecular packing interactions in the solid-state film. Meanwhile, mono- or disubstitution with fluorine causes the ICT bands of **2** and **3** to blueshift by about 18 nm. These results indicate that fluorine substitution of the benzothiadiazole core unit can affect the intermolecular packing interactions more than the amorphous nonplanar TPA in the solid-state film. Moreover, the π–π* transition bands of **2** and **3** were significantly redshifted to by about 30 nm. These redshifts may be due to intermolecular packing through C−F•••H, C−F•••S, or C−F•••π_F interactions in the thin films.[15] To clarify this, attenuated total reflectance (ATR) FTIR spectra of **1–3** were recorded in powder and film states.

The ATR-FTIR spectra of thin films might be expected to provide information on the aggregation of film formation relative to that of powder, as the amorphous solid state of the materials. As shown in Figure 2, the C−F vibrational bands of fluorinated benzothiadiazole could be assigned between 1000 and 1200 cm^{-1} by comparison with unfluorinated BT. Differences between the ATR-FTIR spectra of the thin films and those of films in the powder state indicate packing aggregation in the thin film. Specifically, the fluorinated **bis[TPA-diTh]-BT** derivatives **2** and **3** in thin film form showed somewhat broader peaks at slightly higher wavenumbers compared to the powder state. These results may indicate the state of aggregation, especially H-aggregation, which often results in blueshifts of absorption bands, during formation of the thin film.[16] Also, the higher wavenumber observed in ATR-FTIR spectra of the thin films may indirectly prove the blueshifted absorption spectra in the film state, because the wavenumber is inversely proportional to wavelength.

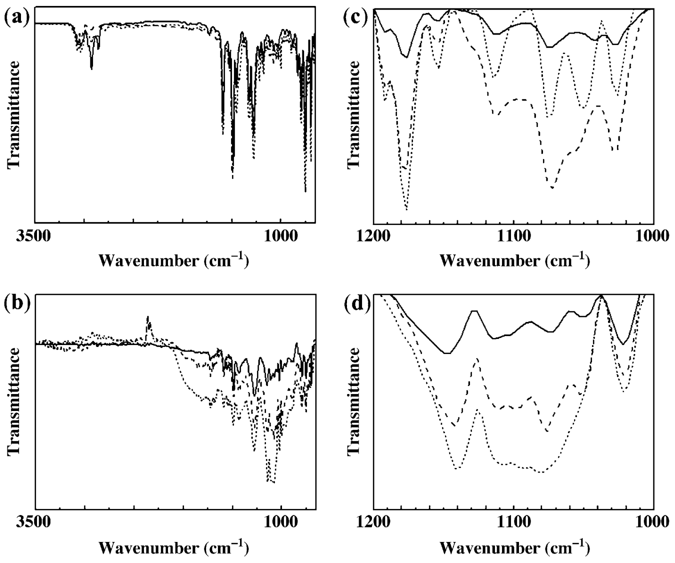

Figure 2. ATR-FTIR spectra of **bis[TPA-diTh]-BT** (black solid line), **bis[TPA-diTh]-MonoF-BT** (dashed line), and **bis[TPA-diTh]-DiF-BT** (short-dashed line) as amorphous solid (a) and spin-cast thin film (b). c) and d) are enlarged regions of a) and b), respectively, from 1200 to 1000 cm^{-1}.

It is also expected that the fluorine atom, which has high electronegativity, will affect the direction and size of the dipole moment of the **bis[TPA-diTh]-BT** derivatives. Figure 3 shows the dipole moments of **1**–**3**, calculated by TD-DFT with the B3LYP functional/6-31G* basis set. The dipole moment of unfluorinated **1** is directed from thiadiazole (δ^+) to benzene ring (δ^-), while this direction is reversed and the value significantly decreased in difluorinated **3**. These results might offset the dipole moment between the TPA donor and BT, resulting in partial H-aggregation, even in an amorphous TPA moiety.

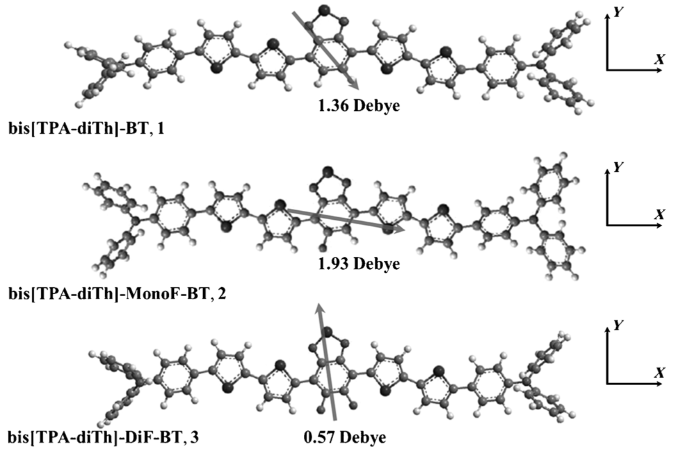

Figure 3. Direction and size of dipole moment of **bis[TPA-diTh]-BT** derivatives **1**, **2**, and **3**, calculated by TD-DFT with the B3LYP functional/6-31G* basis set.

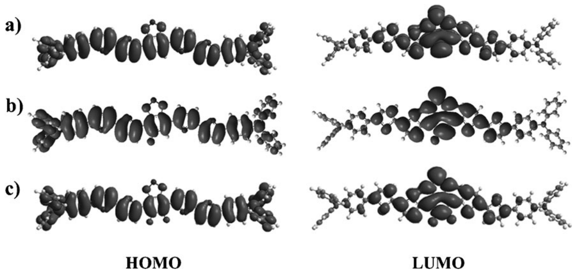

Figure 4. Isodensity surface plots of **1** (a), **2** (b), and **3** (c), calculated by TD-DFT with B3LYP functional/6-21G* basis set.

Figure 4 shows the optimized structures of **1**–**3**, calculated by TD-DFT with the B3LYP functional/6-31G* basis set. The orbital densities of the HOMOs of **1**, **2**, and **3** are evenly distributed on BT–dithophene–TPA, but the orbital density of the LUMO of these materials is predominantly located on BT and fluorine. The calculations revealed that ICT from TPA to BT core can effectively occur in **1**–**3** when excited by light energy, and TPA can play a role in stabilizing separation of the hole from the exciton. In addition, fluoro substituents may provide a more strongly reinforced ICT from TPA to the BT core owing to their electron-withdrawing properties, which results in increased hole mobility due to TPA as a hole stabilizer (see below). Figure 5 shows cyclic voltammograms (CVs) of **1**–**3** in methylene chloride solution, and the corresponding electrochemical properties are summarized in Table 1. The HOMO and the LUMO energy levels of these materials were determined from these CVs. A platinum rod electrode, a platinum wire, and an Ag/AgNO$_3$ (0.10 M) electrode were used as working electrode, counterelectrode, and reference electrode, respectively. The analyses were performed in an electrolyte solution of 0.1 M tetrabutylammonium hexafluorophosphate (TBAPF$_6$) in methylene chloride at room temperature under nitrogen with a scan rate of 100 mV s^{-1}, and ferrocenium/ferrocene (Fc$^+$/Fc) redox couple was used as external reference. The HOMO and LUMO levels can be deduced from the oxidation and reduction onsets under the assumption that the energy level of Fc is 4.8 eV below vacuum level.[17] The CVs of these materials in solid-state thin films could not be measured, owing to film stripping on the electrode. There-

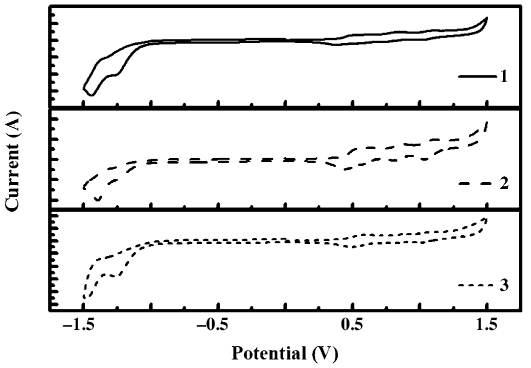

Figure 5. Electrochemical characterization of **1** (top), **2** (middle), and **3** (bottom) in CH$_2$Cl$_2$ with 0.1 M (n-C$_4$H$_9$)$_4$NPF$_6$, scan speed 100 mV s^{-1}.

fore, we determined the bandgaps from solution-state CV. The HOMO levels of **1**, **2**, and **3** were calculated as 5.052, 5.073, and 5.088 eV, and the LUMO levels as 3.686, 3.684, and 3.681 eV, respectively. These results indicate that fluorine substitution on BT slightly reduced the HOMO level of **bis[TPA-diTh]-BT**, which leads to an increase in V_{oc} of devices fabricated by using these materials with PCBM BHJ active layers.[18]

Figure 6a shows the UV/Vis absorption spectra of **1**/C_{71}-PCBM (1/2), **2**/C_{71}-PCBM (1/4), and **3**/C_{71}-PCBM (1/4) films, which exhibited the best performances in BHJ solar cell devices. The ICT bands of **1** and **2** (or **3**) observed in the **1**/C_{71}-PCBM BHJ (1/2) and **2** (or **3**)/C_{71}-PCBM BHJ (1/4) films were similar and blueshifted by about 20 nm, relative to those in solid-state films. These results indicate that the PCBM may significantly interrupt intermolecular π–π packing interactions between p-type organic materials by interacting with the fluorine substituent on the BT moieties of **2** and **3** in the BHJ film.

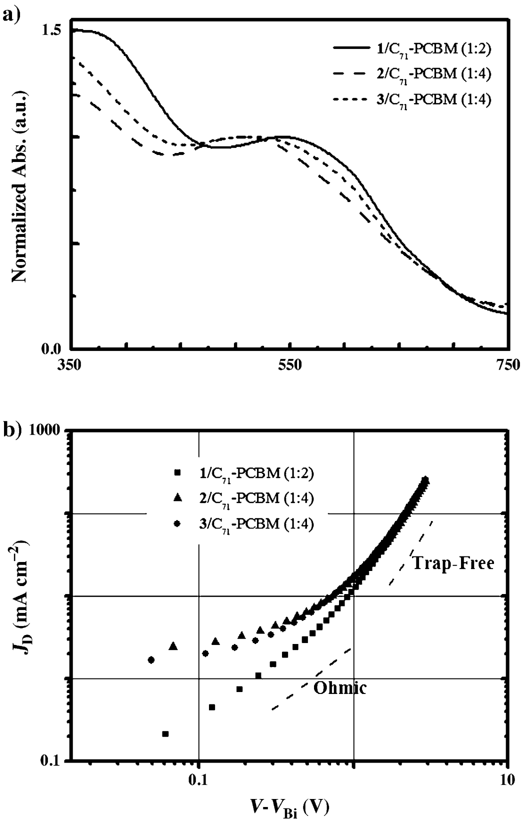

Figure 6. a) UV/Vis absorption spectra and b) space-charge limitation of *J–V* characteristics of **1**/C_{71}-PCBM (1:2) (solid), **2**/C_{71}-PCBM (1:4) (dashed), and **3**/C_{71}-PCBM (1:4) (short-dashed) BHJ films in hole-only devices (ITO/PEDOT:PSS/donor:C_{71}-PCBM/Au).

To investigate the space-charge effects, we extracted the hole mobilities of these organic semiconductors from the space charge limitation of current (SCLC) current–voltage (*J–V*) characteristics obtained in the dark for hole-only devices. Figure 6b shows the dark-current characteristics of ITO/PEDOT:PSS/donor:C_{71}-PCBM/Au devices as a function of the bias, corrected for the built-in voltage determined from the difference in work function between Au and the HOMO level of these materials. Ohm's law manifests at low voltages as an effect of thermal free carriers. In the presence of carrier traps in the active layer, a trap-filled-limit (TFL) region exists between the ohmic and trap-free SCLC regions. The SCLC behavior in the trap-free region can be characterized by using the Mott–Gurney square law [Eq. (1)][19]

$$J = (9/8)\varepsilon \cdot \mu(V^2 L^{-3}) \tag{1}$$

where ε is the static dielectric constant of the medium and μ is the carrier mobility. The hole mobilities of **1**, **2**, and **3** evaluated using the above Mott–Gurney law ($\varepsilon = 3\varepsilon_0$) are 2.14×10^{-6}, 6.62×10^{-6}, and $4.45 \times 10^{-6}\,\mathrm{cm^2V^{-1}s^{-1}}$, respectively. The fluorinated materials **1** and **2** exhibited higher hole mobilities than unfluorinated **1**. Specifically, the hole mobility of monofluorinated **2** was approximately 3 and about 1.5 times higher than those of unfluorinated **1** and difluorinated **3**, respectively. These results suggest that TPA can effectively stabilize the separated hole from the exciton in a BHJ system with PCBM. This reduces charge recombination between the donor and PCBM, and the reinforced ICT due to mono- and difluoro substitution on the BT core may boost the long-lived charge separation and lead to enhanced transporting properties of the hole carrier.

These materials were used for the fabrication of photovoltaic devices along with PCBM BHJ films, and their performances were assessed. In the course of studying the characteristics of more than 500 solar cells, the most efficient photovoltaic cells were obtained from the BHJ system of **1**, **2**, or **3** with C_{71}-PCBM, which were optimized at a ratio of 1:2, 1:4, or 1:4, respectively. These BHJ films were cast on top of a PEDOT:PSS (Heraeus, AI 4083) layer. The optimum thicknesses of **1**/C_{71}-PCBM, **2**/C_{71}-PCBM, and **3**/C_{71}-PCBM BHJ films obtained under these conditions were found to be approximately 80, 85, and 86 nm, respectively. Figure 7 shows the *J–V* curves under AM 1.5 conditions ($100\,\mathrm{mW\,cm^{-2}}$) and incident photon-to-current efficiency (IPCE) spectra of these material/C_{71}-PCBM BHJ solar cells fabricated under optimized processing conditions, with/without insertion of TiO_x, which can effectively act as an optical spacer and buffer layer[20] between the photoactive layer and the Al electrode. The corresponding values are summarized in Table 2.

The IPCE spectra of these devices (Figure 7b) show curves well matched with their optical absorptions, resulting in close correlation with their photocurrents in the *J–V* curves. As shown in Figure 7 and Table 2, the devices conventionally fabricated with **1**/C_{71}-PCBM, **2**/C_{71}-PCBM, and **3**/C_{71}-PCBM exhibited a PCE of 1.62% (±0.2) with a short-circuit current J_{sc} of $7.26\,\mathrm{mA\,cm^{-2}}$, fill factor (FF) of 0.32, and V_{oc} of 0.69 V; a PCE of 2.22% (±0.13) with J_{sc}=

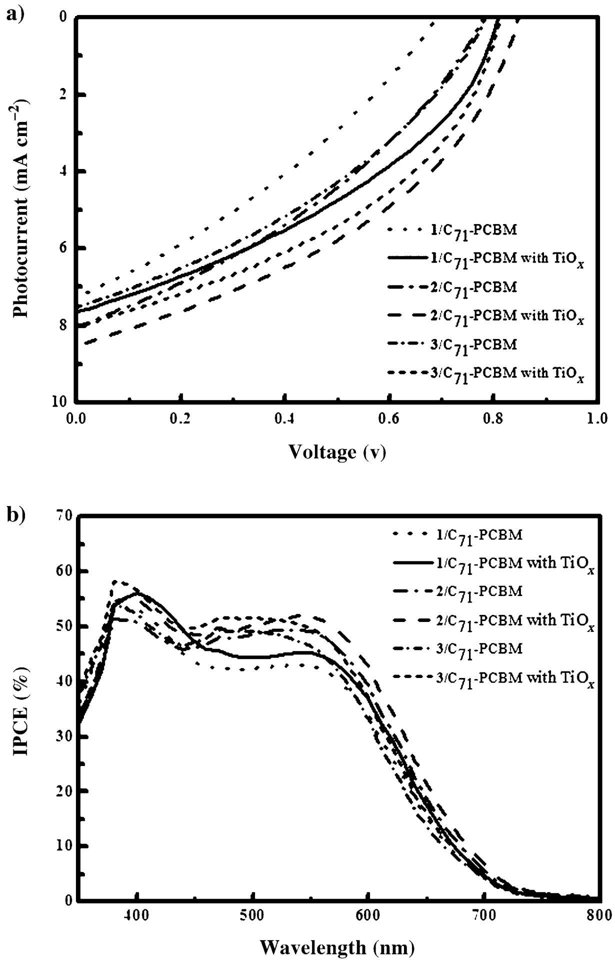

Figure 7. a) J–V curves under AM 1.5 conditions (100 mW cm^{-2}) and b) IPCE spectra of the **1**/C$_{71}$-PCBM (1:2) dotted line), **2**/C$_{71}$-PCBM (1:4) (dash-dotted line), and **3**/C$_{71}$-PCBM (1:4) (short-dash-dotted line) BHJ solar cells fabricated under optimized processing condition with (undotted line)/without (dotted line) insertion of a TiO$_x$ layer.

Table 2. Photovoltaic performances of the devices fabricated with donor (**1**, **2**, or **3**)/C$_{71}$-PCBM BHJ film.[a]

Donor	Functional layer	J_{sc} [mA cm^{-2}]	V_{oc} [V]	FF [%]	E [%]
1	none	7.26	0.69	32	1.62
1	TiO$_x$	7.65	0.81	38	2.38
2	none	8.02	0.78	36	2.22
2	TiO$_x$	8.51	0.85	41	2.95
3	none	7.52	0.79	36	2.14
3	TiO$_x$	8.03	0.81	42	2.74

[a] The optimized BHJ films were spin-cast at 2000 rpm for 60 s. The photovoltaic characteristics were determined under simulated 100 mW cm^{-2} AM 1.5G illumination. The light intensity was calibrated by using calibrated standard silicon solar cells with proactive windows made from KG5 filter glass traced to the National Renewable Energy Laboratory (NREL). The masked active area of the device was 4 mm^2.

8.02 mA cm^{-2}, FF = 0.36, and V_{oc} = 0.78 V; and a PCE of 2.14 % (±0.11) with J_{sc} = 7.52 mA cm^{-2}, FF = 0.36, and V_{oc} = 0.79 V, respectively. The SMOSCs fabricated with **2**/C$_{71}$-PCBM or **3**/C$_{71}$-PCBM BHJ film exhibited better J_{sc} values than that fabricated with **1**/C$_{71}$-PCBM. This was revealed by superior IPCE values in the long-wavelength region, even though the absorption spectra of the **2** (or **3**)/C$_{71}$-PCBM BHJ film showed maximum absorption bands blue-shifted relative to that of **1**/C$_{71}$-PCBM, as shown in Figure 6. The best PCE of 2.95 % (±0.16) was obtained for devices fabricated from a **2**/C$_{71}$-PCBM film with a TiO$_x$ layer (J_{sc} = 8.51 mA cm^{-2}, FF = 0.41, and V_{oc} = 0.85 V), which has about 33 % higher efficiency than that without a TiO$_x$ layer.

Furthermore, compound **2**, containing a monofluorinated BT core, exhibited better photovoltaic performances with higher J_{sc} and V_{oc} than **1** and **3**, which resulted in approximately 24 and 8 % higher efficiencies of SMOSCs, respectively. We also investigated the morphologies of these BHJ films by atomic force microscopy (AFM). Although the BHJ film cast from **1** and PCBM exhibited a slightly higher roughness than those cast from **2** and **3**, there is no obvious difference in the phase-separated morphologies between these BHJ films, all of which show good bicontinuous networks[21] (see Figure S3 in the Supporting Information). As shown in Figure 5, the better efficiency of organic semiconductor with monofluorinated BT is governed by rather high photocurrent compared with that of organic semiconductor with difluorinated BT. Since the surface images of organic semiconductors with mono- or difluorinated BT investigated from AFM analysis both showed good phase-segregated morphologies with similar roughness values, these results may be attributed to the better hole-transporting properties of **2**, as shown in Figure 6.

Conclusion

We have demonstrated the synthesis and photovoltaic characteristics of new fluorine-substituted benzothiadiazole-based compounds **bis[TPA-diTh]-MonoF-BT** (**2**) and **bis-[TPA-diTh]-DiF-BT** (**3**) as efficient p-type organic semiconductors for solution-processed SMOSCs, which showed a PCE of 2.95 % with a V_{oc} of 0.85 V. Moreover, we developed a facile new protocol for the synthesis of mono- or difluorinated BT compounds iodinated at the 4- and 7-positions. These compounds were produced in a single-step reaction by means of a Barker–Waters procedure under relatively mild conditions. These fluorinated **bis[TPA-diTh]-BT** derivatives, which are linked with a TPA electron-donating group through a π-conjugated bithiophene bridge, exhibited reinforced ICT compared to the unfluorinated analogue, in addition to enhanced molar absorptivities.

The unique electronic-repulsive interactions of the fluorine atom affect the intermolecular packing interactions more than the amorphous nonplanar TPA in solid-state film form. Even though these fluorinated SMOSCs exhibited the worst intermolecular interaction, the electron-donating TPA unit could effectively stabilize the hole separated from the exciton in the BHJ system with PCBM to reduce charge recombination between the donor and PCBM. The reinforcement of ICT by mono- and difluoro substitution on the BT core may boost the long-lived charge separation and thus result in improved transporting properties of the hole carrier. The molecular engineering approach demonstrated here provides an important guide for the development of novel materials for use in solution-processed small-molecule BHJ solar cells.

Experimental Section

The BHJ films were prepared under optimized conditions according to the following procedure reported previously.[21] Indium tin oxide (ITO)-coated glass substrate was first cleaned with detergent, ultrasonicated in acetone and isopropyl alcohol, and subsequently dried overnight in an oven. Poly(3,4-ethylenedioxythiophene):polystyrenesulfonate (PEDOT:PSS) in aqueous solution was spun-cast to form a film with thickness of approximately 40 nm. The substrate was dried for 10 min at 140 °C in air, and then transferred into a glove box to spin-cast the photoactive layer. The donor/PCBM BHJ blend solutions were prepared in chlorobenzene at a concentration of 30 mg mL^{-1}, and then spun-cast on top of the PEDOT layer. Then, the device was pumped down to less than 10^{-7} torr and an approximately 100 nm thick Al electrode was deposited on top. Solar cell efficiencies were characterized under simulated 100 mW cm^{-2} AM 1.5G irradiation from a 1000 W Xe arc lamp (Oriel 91193). The light intensity was adjusted with a Si solar cell that was double-checked with an NREL-calibrated Si solar cell (PV Measurement Inc.). The applied potential and measured cell current were measured with a Keithley model 2400 digital source meter. The current–voltage characteristics of the cell under these conditions were determined by biasing the cell externally and measuring the generated photocurrent. This process was fully automated by using Wavemetrics software. The IPCE spectra for the cells were measured on an IPCE measuring system (PV measurements).

Acknowledgements

This research was supported by World Class University program funded by the Ministry of Education, Science and Technology through the National Research Foundation of Korea (R31-2011-000-10035-0), the Converging Research Center Program through the Ministry of Education, Science and Technology (No. 2011K000596) and the New & Renewable Energy of the Korea Institute of Energy Technology Evaluation ad Planning (KETEP) grant funded by the Korea government Ministry of Knowledge Economy (no. 20103060010020).

---

[1] a) D. Demeter, T. Rousseau, P. Leriche, T. Cauchy, R. Po, J. Roncali, *Adv. Funct. Mater.* **2011**, *21*, 4379–4387; b) B. Walker, C. Kim, T.-Q. Nguyen, *Chem. Mater.* **2011**, *23*, 470–482.

[2] M. A. Green, K. Emery, Y. Hishikawa, W. Warta, E. D. Dunlop, *Prog. Photovoltaics* **2011**, *19*, 565–572.

[3] S. C. Price, A. C. Stuart, L. Yang, H. Zhou, W. You, *J. Am. Chem. Soc.* **2011**, *133*, 4625–4631.

[4] a) S. Roquet, A. Cravino, P. Leriche, O. Alévêque, P. Frère, J. Roncali, *J. Am. Chem. Soc.* **2006**, *128*, 3459–3466; b) A. Cravino, P. Leriche, O. Aleveque, S. Roquet, J. Roncali, *Adv. Mater.* **2006**, *18*, 3033–3037; c) A. B. Tamayo, X. D. Dang, B. Walker, J. Seo, T. Kent, T. Q. Nguyen, *Appl. Phys. Lett.* **2009**, *94*, 103301; d) C. Q. Ma, M. Fonrodona, M. C. Schikora, M. M. Wienk, R. A. J. Janssen, P. Bauele, *Adv. Funct. Mater.* **2008**, *18*, 3323–3331; e) Z. E. Ooi, T. L. Tam, R. Y. C. Shin, Z. K. Chen, T. Kietzke, A. Sellinger, M. Baumgarten, K. Mullen, J. C. deMello, *J. Mater. Chem.* **2008**, *18*, 4619–4622; f) J. Lee, M. H. Yun, J. Kim, J. Y. Kim, C. Yang, *Macromol. Rapid Commun.* **2012**, *33*, 140–145; g) J. Lee, J. Kim, G. Kim, C. Yang, *Tetrahedron* **2010**, *66*, 9440–9444.

[5] Y. Sun, G. C. Welch, W. L. Leong, C. J. Takacs, G. C. Bazan, A. J. Heeger, *Nat. Mater.* **2011**, *11*, 44–48.

[6] a) H. M. Ko, H. Choi, S. Paek, K. Kim, K. Song, J. K. Lee, J. Ko, *J. Mater. Chem.* **2011**, *21*, 7248–7253; b) B. S. Jeong, H. Choi, N. Cho, H. M. Ko, W. Lim, K. Song, J. K. Lee, J. Ko, *Sol. Energy Mater. Sol. Cells* **2011**, *95*, 1731–1740; c) S. So, H. Choi, C. Kim, N. Cho, H. M. Ko, J. K. Lee, J. Ko, *Sol. Energy Mater. Sol. Cells* **2011**, *95*, 3433–3441; d) S. So, H. Choi, H. M. Ko, C. Kim, S. Paek, N. Cho, K. Song, J. K. Lee, J. Ko, *Sol. Energy Mater. Sol. Cells* **2012**, *98*, 224–232; e) H. Choi, S. Paek, J. Song, C. Kim, N. Cho, J. Ko, *Chem. Commun.* **2011**, *47*, 5509–5511.

[7] H. Zhou, L. Yang, A. C. Stuart, S. C. Price, S. Liu, W. You, *Angew. Chem.* **2011**, *123*, 3051–3054; *Angew. Chem. Int. Ed.* **2011**, *50*, 2995–2998.

[8] Y. Zhang, S. C. Chien, K. S. Chen, H. L. Yip, Y. Sun, J. A. Davices, F. C. Chen, A. K. Y. Jen, *Chem. Commun.* **2011**, *47*, 11026–11028.

[9] a) Y. Y. Liang, D. Q. Feng, Y. Wu, S. T. Tsai, G. Li, C. Ray, L. P. Yu, *J. Am. Chem. Soc.* **2009**, *131*, 7792–7799; b) Q. Wei, T. Nishizawa, K. Tajima, K. Hashimoto, *Adv. Mater.* **2008**, *20*, 2211–2216.

[10] S.-J. Moon, J.-H. Yum, R. Humphry-Baker, K. M. Karlsson, D. P. Hagberg, T. Marinado, A. Hagfeldt, L. Sun, M. Gratzel, Md. K. Nazeeruddin, *J. Phys. Chem. C* **2009**, *113*, 16816–16820.

[11] I. R. L. Barker, W. A. Waters, *J. Chem. Soc.* **1952**, 150–153.

[12] J. Bouffard, T. M. Swager, *Macromolecules* **2008**, *41*, 5559–5562.

[13] W. Li, C. Du, F. Li, Y. Zhou, M. Fahlman, Z. Bo, F. Zhang, *Chem. Mater.* **2009**, *21*, 5327–5334.

[14] a) R. C. Coffin, J. Peet, J. Rogers, G. C. Bazan, *Nat. Chem.* **2009**, *1*, 657–661; b) A. Leliège, P. Blanchard, T. Rousseau, J. Roncali, *Org. Lett.* **2011**, *13*, 3098–3101.

[15] Y. Wang, S. R. Parkin, J. Gierschner, M. D. Watson, *Org. Lett.* **2008**, *10*, 3307–3310.

[16] F. Nüetsch, J. E. Moser, V. Shklover, M. Grätzel, *J. Am. Chem. Soc.* **1996**, *118*, 5420–5431.

[17] a) J. Pommerehene, H. Vestweber, W. Guss, R. F. Mahrt, H. Bässler, M. Porsch, J. Daub, *Adv. Mater.* **1995**, *7*, 551–554; b) Z. Chen, M. G. Debije, T. Debaerdemaeker, P. Osswald, F. Würthner, *ChemPhysChem* **2004**, *5*, 137–140.

[18] M. C. Scharber, D. Mühlbacher, M. Koppe, P. Denk, C. Waldauf, A. J. Heeger, C. J. Brabec, *Adv. Mater.* **2006**, *18*, 789–794.

[19] V. D. Mihailetchi, H. Xie, B. Boer, L. J. A. Koster, P. W. M. Blom, *Adv. Funct. Mater.* **2006**, *16*, 699–708.

[20] K. Lee, J. Y. Kim, S. H. Park, S. H. Kim, S. Cho, A. J. Heeger, *Adv. Mater.* **2007**, *19*, 2445–2449.

[21] J. K. Lee, W. L. Ma, C. J. Brabec, J. Yuen, J. S. Moo, J. Y. Kim, K. Lee, G. C. Bazan, A. J. Heeger, *J. Am. Chem. Soc.* **2008**, *130*, 3619–3623.

Received: April 19, 2012
Revised: May 25, 2012

Organic Semiconductors

*N. Cho, K. Song, J. K. Lee,**
*J. Ko** .... ■■■■–■■■■

Facile Synthesis of Fluorine-Substituted Benzothiadiazole-Based Organic Semiconductors and Their Use in Solution-Processed Small-Molecule Organic Solar Cells

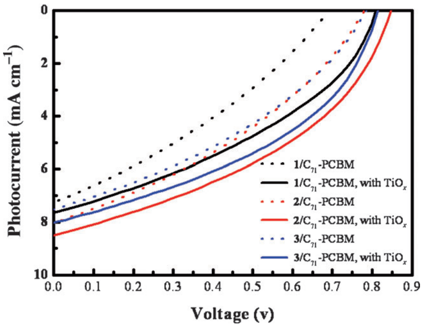

A facile new protocol was developed for synthesis of iodinated derivatives of fluorinated benzothiadiazoles as precursors for fluorine-substituted benzothiadiazole-based organic semiconductors **2** and **3**, which exhibit enhanced intramolecular charge transfer compared to unfluorinated analogue **1** and hence improved photovoltaic performance in small-molecule organic solar cells (see figure).